Title
Exploring a multi-scale method for molecular simulation in continuum solvent model: Explicit simulation of continuum solvent as an incompressible fluid

Journal
The Journal of Chemical Physics, 147(21)

ISSN
0021-9606

Authors
Xiao, Li
Luo, Ray

Publication Date
2017-12-07

DOI
10.1063/1.5016052

Peer reviewed

Exploring a multi-scale method for molecular simulation in continuum solvent model: Explicit simulation of continuum solvent as an incompressible fluid

Li Xiao[1,2] and Ray Luo[1,2,3,a)]
[1]*Departments of Biomedical Engineering, University of California, Irvine, California 92697, USA*
[2]*Molecular Biology and Biochemistry, University of California, Irvine, California 92697, USA*
[3]*Chemical Engineering and Materials Science, University of California, Irvine, California 92697, USA*

(Received 24 April 2017; accepted 15 November 2017; published online 7 December 2017)

We explored a multi-scale algorithm for the Poisson-Boltzmann continuum solvent model for more robust simulations of biomolecules. In this method, the continuum solvent/solute interface is explicitly simulated with a numerical fluid dynamics procedure, which is tightly coupled to the solute molecular dynamics simulation. There are multiple benefits to adopt such a strategy as presented below. At this stage of the development, only nonelectrostatic interactions, i.e., van der Waals and hydrophobic interactions, are included in the algorithm to assess the quality of the solvent-solute interface generated by the new method. Nevertheless, numerical challenges exist in accurately interpolating the highly nonlinear van der Waals term when solving the finite-difference fluid dynamics equations. We were able to bypass the challenge rigorously by merging the van der Waals potential and pressure together when solving the fluid dynamics equations and by considering its contribution in the free-boundary condition analytically. The multi-scale simulation method was first validated by reproducing the solute-solvent interface of a single atom with analytical solution. Next, we performed the relaxation simulation of a restrained symmetrical monomer and observed a symmetrical solvent interface at equilibrium with detailed surface features resembling those found on the solvent excluded surface. Four typical small molecular complexes were then tested, both volume and force balancing analyses showing that these simple complexes can reach equilibrium within the simulation time window. Finally, we studied the quality of the multi-scale solute-solvent interfaces for the four tested dimer complexes and found that they agree well with the boundaries as sampled in the explicit water simulations. *Published by AIP Publishing.* https://doi.org/10.1063/1.5016052

I. INTRODUCTION

Atomistic simulation has become an important tool for studying the structures, dynamics, and functions of biomolecular systems. Nevertheless efficient atomistic simulation of large and complex biomolecular systems is still one of the remaining challenges in computational molecular biology. The computational challenges in atomistic simulation of biomolecular systems are direct consequences of their high dimensionalities. Indeed biomolecules are highly complex molecular machines with thousands to millions of atoms. What further complicates the picture is the need to realistically treat the interactions between biomolecules and their surrounding water molecules that are ubiquitous and of paramount importance for their structures, dynamics, and functions.

Since most particles in biomolecular simulations are to represent water molecules solvating the target biomolecules, an implicit treatment of water molecules allows greatly increased simulation efficiency. Indeed, implicit solvation offers a unique opportunity for more efficient simulations without the loss of atomic-level resolution for biomolecules.[1–17] Advance in implicit solvation, coupled with developments in sampling algorithms, classical force fields, and quantum approximations, will prove useful to the larger biomedical community in a broad range of studies of biomolecular structures, dynamics, and functions.

One class of implicit solvent models, the classical Poisson-Boltzmann solvent model, has become widely accepted in biomolecular applications after over 30 years of basic research and development. Efficient numerical PB equation (PBE)-based solvent models have been widely used to study biological processes.[18–42] However, challenges remain to achieve more consistent, accurate, and robust analysis of biomolecules.[43–60] The existing dielectric model based on molecular solvent excluded surface is a major hurdle for applications of the PBE solvent models. This dielectric model is *ad hoc*, expensive, and numerically unstable due to its treatment of atoms as hard spheres in molecular simulations. Efforts to improve the simple dielectric model have emerged to describe the physical location of the boundary and to model the heterogeneous dielectric response of the interfacial liquid.[61,62] Nevertheless, we also see more pressing needs in incorporating the classical PBE models in molecular dynamics (MD)/free energy simulations. Indeed, existing approximated approaches, such as the molecular mechanics Poisson-Boltzmann surface area method that is currently widely used in the community, cannot be used to dissect any

a)Author to whom correspondence should be addressed: ray.luo@uci.edu

proposed improvements of classical PBE models due to their approximations and intrinsic errors.

In this study, we intend to explore a multi-scale simulation algorithm for the classical PBE models to explicitly simulate the continuum solvent/solute interface with the solvent fluid dynamics (FD) that is coupled to the solute molecular dynamics. This algorithm allows a self-consistent treatment of the solvation interactions, i.e., the dielectric interface automatically adjusts to local conformational and energetic fluctuations and is guaranteed to be at the system free energy minimum upon equilibrium, so that it naturally addresses the limitation of the current dielectric model.[61,62] In addition, our algorithm was developed with the goal of better utilization of the PBE model in molecular dynamics simulations, in that it (1) allows a "soft" and physical dielectric interface for stable dynamics; (2) eliminates atom-specific cavity radii that must be defined, dramatically reducing the freely adjustable parameters of the PBE treatment; (3) eliminates the expensive molecular surface reconstruction step during dynamics; and (4) eliminates the difficult and expensive molecular surface-to-atom mapping of dielectric boundary forces and hydrophobic boundary forces and applies these surface forces to the continuum solvent instead. The multi-scaled simulation method utilizes a 3D numerical algorithm previously developed to solve the Navier-Stokes (NS) equation.[63,64] It should be pointed out that the use of Navier-Stokes equation, instead of the Stokes equation that is sufficient for biomolecular processes of interest, is necessary for the lack of a predefined solute-solvent interface, or in a "free-boundary" problem.[63,64]

This manuscript documents our initial effort in the construction of the multi-scale algorithm. Specifically, we incorporated the fluid dynamics algorithm into the Amber molecular mechanics simulation engine[65–67] and assessed the quality of the solvent-solute interface simulated for several simple biomolecular systems and compared with explicit solvent simulations. It should be pointed out that we are mainly interested in equilibrium properties of the biomolecular solute in the development of the algorithm, and solvent hydrodynamics is not our consideration. Thus certain alterations of the fluid dynamics algorithm can be utilized to artificially accelerate the solvent relaxation process so that the precious computing resources can be focused on sampling of solute conformations.

II. THEORY

In the following, we first review our physical model for easy understanding of the overall approach. Next we briefly go over the fluid dynamics algorithm and procedure with a focus on how to adapt the method to atomistic molecular simulations. Finally computational details are presented for the numerical tests of specific molecular systems.

A. Physical model

Our basic model is derived from the Hamiltonian equation. A Hamiltonian for the entire system is thus defined first. Its degrees of freedom are atomic positions (x) and their velocities (v) for the solute molecular dynamics (MD) region and fluid element displacements (y) and their velocities (u) for the solvent fluid dynamics (FD) region. For the MD region, all-atom molecular mechanics will be used. Molecular mechanics usually adopts a relatively simple potential energy function, or force field, for efficient computation. Many potential energy functions have been developed for biomolecular applications, such as Amber,[68–73] CHARMM,[74–76] and OPLS.[77–79] For the FD region, an incompressible viscous fluid model is adopted.

The Hamiltonian is defined as

$$H = H_{\mathrm{MD}}(x, \alpha_x) + H_{\mathrm{MD/FD}}(x, \alpha_x; y, \alpha_y) + H_{\mathrm{FD}}(y, \alpha_y), \quad (1)$$

where α_x is the momentum of the MD region and α_y is the momentum of the FD region. H_{MD} is the Hamiltonian of for the MD region modeled by molecular mechanics $H_{\mathrm{MD}} = U + K$, where U is the force field potential energy and K is the kinetic energy. $H_{\mathrm{MD/FD}} = U_{ele} + U_{vdw}$ consists of two terms. U_{ele} is the Poisson-Boltzmann electrostatic solvation energy.[16,60,80,81] The nonelectrostatic solvation energy is usually modeled as two components: the van der Waals component U_{vdw} and the hard sphere entropy/cavity component U_{hse}.[82–86] However, different from all-particle simulation methods, the U_{hse} term is now a component in the FD region as is discussed below. Here U_{ele} is defined as

$$\begin{aligned} U_{ele} &= \int \left(\rho^f \phi - \frac{1}{8\pi} D \cdot E - \Delta\Pi\lambda\right) dV, \\ \Delta\Pi &= kT \sum_i c_i (e^{-q_i\phi/kT} - 1), \end{aligned} \quad (2)$$

in the classical PBE model. U_{vdw} is defined as

$$U_{vdw} = \sum_{a=1}^{N_s} \int \rho_{aw}(r_{aw}) u_{\mathrm{LJ}}(r_{aw}) dV, \quad (3)$$

where the sum is over all solute atoms (N_s) and the integration is over the solvent-occupied volume. $\rho_{aw}(r_{aw})$ is a solvent distribution function around a solute atom "a" at a given solute-solvent distance. $u_{\mathrm{LJ}}(r) = \frac{A}{r^{12}} - \frac{B}{r^6}$ is the force field Lennard-Jones potential given the coefficients A and B for each atom. Finally, H_{FD} represents the Hamiltonian for the incompressible solvent fluid, with the form

$$H_{\mathrm{FD}} = \int \left[\frac{1}{2}\rho u^2 + U_{\mathrm{int}}(\rho, s)\right] dV + \int \gamma dA + c, \quad (4)$$

where ρ is the fluid density, s is the entropy density, $\frac{1}{2}\rho u^2$ is the kinetic energy density, and U_{int} is the internal energy density.[87] Note that

$$U_{hse} = \int \gamma dA + c, \quad (5)$$

where γ is the surface tension and c is an offset constant, is the second component of the nonelectrostatic solvation free energy. Here the surface integration is over all interfaces of the FD region. Since the fluid is infinitely large, the only interface concerning us is that with the particle solute. The interface identification and the surface integration, also known as the surface area as γ is constant, are numerically implemented with the level set method and are presented in Sec. III.

Now we proceed to derive the dynamics equation by first using a shorthand notation of $\beta = (x, y)$ as the position vector

of the system and $\alpha = (\alpha_x, \alpha_y)$ as the momentum vector of the system. The familiar Newtonian dynamics can be derived from Hamilton's equation as

$$\dot{\alpha} = -\frac{\partial H}{\partial \beta}. \tag{6}$$

Here we have adopted the convention that α and β represent the moment and position vectors of each particle/element, respectively.

In the molecule dynamics region, the equation of motion for an atom at position vector x can be expressed symbolically as

$$\dot{\alpha}_x = -\frac{\partial H_{\mathrm{MD}}}{\partial x} - \frac{\partial H_{\mathrm{MD/FD}}}{\partial x}. \tag{7}$$

$-\frac{\partial H_{\mathrm{MD}}}{\partial x}$ represents the usual force field terms in molecule dynamics simulations. The coupling Hamiltonian has two terms, $U_{ele} + U_{vdw}$, so the coupling force terms that the atoms feel are only those of electrostatics and van der Waals in nature, i.e., $-\frac{\partial H_{\mathrm{MD/FD}}}{\partial x} = -\frac{\partial U_{ele}}{\partial x} - \frac{\partial U_{vdw}}{\partial x}$. It is interesting to note that the electrostatic forces $-\frac{\partial U_{ele}}{\partial x}$ are simply the qE forces on atomic point charges in a force field model.[60] $-\frac{\partial U_{vdw}}{\partial x}$ are the van der Waals forces from the solvent molecules modeled as continuum.[84]

In the fluid dynamics region, consider a small fluid volume element at position y, with volume V and velocity u. The equation of motion of the fluid element is

$$\dot{\alpha}_y = -\frac{\partial H_{\mathrm{FD}}}{\partial y} - \frac{\partial H_{\mathrm{MD/FD}}}{\partial y}. \tag{8}$$

As shown below, the variational principle is applied to this element. The partial derivative can also be written in the variational form as

$$\dot{\alpha}_y = -\frac{\delta H_{\mathrm{FD}}}{\delta y}\Big|_u - \frac{\delta H_{\mathrm{MD/FD}}}{\delta y}\Big|_u. \tag{9}$$

Here the subscript u denotes that it is fixed during the variation. Notice here that $y = y(q, t)$ is the Lagrangian coordinate of the volume element, which is fixed on the fluid element and q is introduced here to denote the actual spatial position.[87] In this subsection, we consider an interior fluid volume element, i.e., an element not on the interface, to derive the equations of motion for the fluid interior. In Sec. II B, we will focus on an interface element to derive the boundary conditions.

To proceed we impose a variation δy on the element within time dt to compute the variation of H_{FD}. Since the element is not on the interface, U_{hse} does not change under its variation, so we can focus on the first two terms of H_{FD} only. The process is also assumed to be very rapid, i.e., $\frac{\delta y}{dt} \gg 0$.

Since the fluid is incompressible, $\nabla\cdot\delta y = 0$, the work done to the environment of the element is[87]

$$\begin{aligned} dW = \int p\delta y \cdot dA &= \int \nabla\cdot(p\delta y)dV \\ &= \int \nabla p\cdot\delta y dV + \int p\nabla\cdot\delta y dV \\ &= \int \nabla p\cdot\delta y dV, \end{aligned} \tag{10}$$

where p is the pressure and vector dA denotes the area of the surface element with the direction along the normal of the surface element. Given that the first and second laws of thermodynamics still hold, the internal energy variation can be expressed as[87]

$$\int \delta U_{\mathrm{int}} dV = \int (T\delta s)dV - dW = \int (T\delta s)dV - \int \nabla p\cdot\delta y dV. \tag{11}$$

The second law provides a constraint for the entropy variation as

$$\int (T\delta s)dV = \int f_{vis}\cdot\delta y dV - dt\int \nabla\cdot Q dV, \tag{12}$$

where Q is the heat flux and f_{vis} is the viscous force density. Given the fact that the term involving dt can be ignored as $\frac{\delta y}{dt} \gg 0$, substitution of Eq. (12) into Eq. (11) leads to the variation of the internal energy as

$$\int \delta U_{\mathrm{int}} dV = \int (f_{vis}\cdot\delta y)dV - \int \nabla p\cdot\delta y dV = \int (f\cdot\delta y)dV. \tag{13}$$

Here the total force density $f = f_{vis} - \nabla p = \frac{\partial \sigma_{ij}}{\partial y_j}$ is introduced, where $\sigma_{ij} = -p\delta_{ij} + \mu\left(\frac{\partial u_i}{\partial y_j} + \frac{\partial u_j}{\partial y_i}\right)$ is defined as the stress tensor and μ is the fluid viscosity constant.[88] Given the assumption that the force density is uniform within the volume element, substitution of Eq. (13) into the variation of H_{FD} gives

$$-\frac{\delta H_{\mathrm{FD}}}{\delta y}\Big|_u = -\frac{\int \delta U_{\mathrm{int}} dV}{\delta y} = -fV = -\frac{\partial \sigma_{ij}}{\partial y_j}V. \tag{14}$$

The variation of $H_{\mathrm{MD/FD}}$ is presented next. In Poisson-Boltzmann systems with mobile ions, there is an ionic force term at the Stern layer,[60] but it is usually much smaller than other force terms and is often ignored. If it were not ignored, the ionic force would act upon relevant volume elements. Thus the only significant derivative of $H_{\mathrm{MD/FD}}$ is the van der Waals force, which can be treated as the "external force" density (F) on the fluid element, i.e.,

$$-\frac{\delta H_{\mathrm{MD/FD}}}{\delta y}\bigg|_u = -\frac{\delta U_{vdw}}{\delta y} = FV. \tag{15}$$

Finally, the change of momentum of the fluid volume element is

$$\begin{aligned} \dot{\alpha}_y = \frac{d(\rho V u)}{dt} &= \rho V\frac{\partial u}{\partial t} + \sum_i \rho V\frac{\partial u}{\partial q_i}\frac{\partial q_i}{\partial t} \\ &= \rho V\frac{\partial u}{\partial t} + \rho V(u\cdot\nabla)u. \end{aligned} \tag{16}$$

Combination of Eqs. (8) and (14)–(16) gives[87]

$$\rho V\frac{\partial u}{\partial t} + \rho V(u\cdot\nabla)u = \frac{\partial \sigma_{ij}}{\partial y_j}V + FV. \tag{17}$$

This becomes the incompressible Navier-Stokes equation after removing the common volume factor and spelling out the stress tensor (σ_{ij}),

$$\rho\left(\frac{\partial u}{\partial t} + (u\cdot\nabla)u\right) = -\nabla p + \mu\Delta u + F. \tag{18}$$

The conservation of volume/mass, $\nabla\cdot u = 0$, is often written together with Eq. (18) to show it is for the incompressible fluid.

B. Derivation of interface conditions

To obtain the interface conditions, an infinitely small disk-like fluid volume element ε is introduced with small area A and thickness h, with $h \ll \sqrt{A}$. The disk surfaces are parallel to the boundary interface and one side of the surface is right next to the molecule dynamics region. Given a variation of the disk position with δy_ε,

$$\dot{\alpha}_\varepsilon = -\frac{\delta H_{\mathrm{FD}}}{\delta y_\varepsilon} - \frac{\delta H_{\mathrm{FD/MD}}}{\delta y_\varepsilon}. \tag{19}$$

The left-hand side can be computed as

$$\dot{\alpha}_\varepsilon = \rho A h \frac{du}{dt}, \tag{20}$$

which is proportional to the disk element volume, Ah, and can be ignored as h is infinitely small. To compute the right-hand side, we first introduce the local coordinate system, which consists of one normal direction (n) and two tangential directions (t, τ) at a certain point on the interface, i.e.,

$$\begin{cases} n = \cos\alpha_1 i + \cos\alpha_2 j + \cos\alpha_3 k \\ t = \cos\beta_1 i + \cos\beta_2 j + \cos\beta_3 k \\ \tau = \cos\gamma_1 i + \cos\gamma_2 j + \cos\gamma_3 k \end{cases}. \tag{21}$$

Stress $-\frac{\delta H_{\mathrm{FD}}}{\delta y_\varepsilon}$ only exerts on the disk surface in the fluid region so that

$$\begin{aligned} -\frac{\delta H_{\mathrm{FD}}}{\delta y_\varepsilon} &= \sigma_{ij}\cdot nA - \frac{\partial U_{hse}}{\partial y_\varepsilon} \\ &= \left[\left(-p + 2\mu\frac{\partial u_n}{\partial n}\right)n + \mu\left(\frac{\partial u_n}{\partial t} + \frac{\partial u_t}{\partial n}\right)t \right. \\ &\quad \left. + \mu\left(\frac{\partial u_n}{\partial \tau} + \frac{\partial u_t}{\partial n}\right)\tau\right]A - \frac{\partial U_{hse}}{\partial y_\varepsilon}. \end{aligned} \tag{22}$$

The term $-\frac{\partial U_{hse}}{\partial y_\varepsilon} = -\gamma\kappa An$ is the surface tension from the hard sphere entropy, also known as the hydrophobic term,[84] where κ is the curvature. The last term in Eq. (19) can be worked out as

$$-\frac{\delta H_{\mathrm{MD/FD}}}{\delta y_\varepsilon} = -\frac{\delta U_{ele}}{\delta y_\varepsilon} - \frac{\delta U_{vdw}}{\delta y_\varepsilon}, \tag{23}$$

where $-\frac{\partial U_{ele}}{\partial y_\varepsilon} = f_{dielec}A = \frac{1}{2}\sigma^{pol}\frac{D^i\cdot D^o}{D_n^o}An$ is the dielectric boundary force.[60] The van der Waals force, $\frac{\delta U_{vdw}}{\delta y_\varepsilon}$, proportional to the disk element volume Ah, can be ignored when comparing to the electrostatic forces and surface tension. Combining Eqs. (19) and (20) and the terms calculated above, the interface conditions can be summarized as

$$\begin{aligned} -p - \gamma\kappa + 2\mu\frac{\partial u_n}{\partial n} + f_{dielec} &= 0, \\ \frac{\partial u_n}{\partial t} + \frac{\partial u_t}{\partial n} &= 0, \\ \frac{\partial u_n}{\partial \tau} + \frac{\partial u_t}{\partial n} &= 0, \end{aligned} \qquad \text{on } \partial\Omega. \tag{24}$$

III. NUMERICAL ALGORITHMS

We explored to implement the multi-scale algorithm in numerical simulations with a strategy similar to those of the classical Car-Parrinello molecular dynamics (CPMD) method,[89] which can be regarded as a multi-scale algorithm via coupling equations of motion for ions and electrons in two different mechanics. In CPMD, electrons are treated as active degrees of freedom, via fictitious dynamics variable, and the fictitious electron dynamics is coupled with ionic dynamics in the Berendsen heat bath to approach the Born-Oppenheimer surface. The CPMD method results in a conservative ionic dynamics that is extremely close to the Born-Oppenheimer surface.

Our approach is to couple equations of motion for solute atoms and continuum solvent. The solvent part is also treated by the fictitious dynamics variable, and since our method is based on a finite-difference method, it is the fluid element. The fictitious fluid dynamics is modeled by the incompressible Navier-Stokes (NS) equation. The fictitious fluid dynamics model is coupled with the all-atom molecular dynamics model in the Berendsen heat bath to approach the surface provided by all-atom MD simulations at a preset temperature. In doing so, the changes to the existing molecular mechanics simulation engine can be kept at the minimal and there is a very clear boundary between the FD and MD simulation routines, facilitating the development of the new algorithm into a viable simulation engine for future biomolecular applications.

A. FD time integration

Our previous work has addressed the mathematical issues in solving fluid dynamics equations numerically.[63,64] After setting the water density to unity, the velocity can be solved by the second-order semi-implicit backward Euler method as

$$\begin{aligned} \frac{3u^{k+1} - 4u^k + u^{k-1}}{2\Delta t} + (u\cdot\nabla u)^{k+1} \\ = -\nabla p^{k+1} + \mu\Delta u^{k+1} + F^{k+1}, \textit{outside}, \\ \frac{3u^{k+1} - 4u^k + u^{k-1}}{2\Delta t} = \mu\Delta u^{k+1}, \textit{inside}, \end{aligned} \tag{25}$$

where

$$\begin{aligned} p^{k+1} &= 2p^k - p^{k-1}, \\ (u\cdot\nabla u)^{k+1} &= 2(u\cdot\nabla u)^k - (u\cdot\nabla u)^{k-1}. \end{aligned} \tag{26}$$

The pressure is solved by

$$\Delta p^{k+1} = -\nabla\cdot((u^{k+1}\cdot\nabla)u^{k+1}) + \nabla\cdot F^{k+1}. \tag{27}$$

A new issue facing the application of the FD simulation to molecular systems is the presence of van der Waals force (F), which has a large gradient nearby the interface because it is too close to the solute atom centers. The large gradient is almost always challenging to address with a finite-difference type of method. In this study, we overcome the issue by introducing a variable p', where $p' = p + \Gamma$ with $\nabla\Gamma = -F$ is obtained analytically. Therefore, we can solve $\nabla p' = \mu\Delta u$ without computing the numerical gradient of the van der Waals potential. Specifically given $p'^{(k+1)} = p^{k+1} + \Gamma^{k+1}$, the equivalent form in Eq. (27) is to be solved numerically as

$$\Delta p'^{(k+1)} = -\nabla\cdot((u^{k+1}\cdot\nabla)u^{k+1}). \tag{28}$$

Accordingly, Eq. (25) is updated as

$$\begin{aligned}&\frac{3u^{k+1}-4u^k+u^{k-1}}{2\Delta t}+(u\cdot\nabla u)^{k+1}\\&\quad=-\nabla p'^{(k+1)}+\mu\Delta u^{k+1},\ outside\\&\frac{3u^{k+1}-4u^k+u^{k-1}}{2\Delta t}=\mu\Delta u^{k+1},\ inside,\end{aligned}\tag{29}$$

where $p'^{(k+1)}$ is taken as

$$p'^{(k+1)}=2p'^{(k)}-p'^{(k-1)}.\tag{30}$$

Finally the interface boundary condition equation (24) becomes

$$\begin{aligned}-p'+\Gamma-\gamma\kappa+2\mu\frac{\partial u_n}{\partial n}&=0,\\\frac{\partial u_n}{\partial t}+\frac{\partial u_t}{\partial n}&=0,\\\frac{\partial u_n}{\partial \tau}+\frac{\partial u_t}{\partial n}&=0.\end{aligned}\tag{31}$$

At each time step, p' is interpolated with the one-side least square fitting method.[50] Γ is computed analytically for each interface point where the interface boundary condition equation (31) is enforced. When doing so, we can completely avoid finite-difference operations involving van der Waals energy and forces.

As presented in our previous studies, the remaining major mathematical challenge in solving these coupled partial differential equations is the presence of the free-boundary condition equation (24) that allows the solute-solvent interface to equilibrate according to our physical model. To enforce the free-boundary condition when solving pressure or velocity, we utilized the jump conditions of u_n and p as the augmented variables, respectively.[63,64,90] The considerations of augmented variables lead to extra correction terms on the right-hand side in Eqs. (25) and (27). After the correction, each velocity component solver is equivalent to a Helmholtz equation. Once the velocity is updated, the pressure solver is simplified to a Poisson equation. In this implementation, we utilized the modified incomplete Cholesky conjugate gradient numerical solver to solve these linear differential equations.[91–94]

When solving the linear systems, the fluid domain is contained in a rectangular box, and the conditions at the outer boundary of the rectangular R are

$$\begin{aligned}u|_{x=x_{\min}}&=0,\ u|_{x=x_{\max}}=0,\\\left.\frac{\partial u}{\partial y}\right|_{y=y_{\min}}&=0,\ \left.\frac{\partial u}{\partial y}\right|_{y=y_{\max}}=0,\qquad \text{on } \partial R,\\u|_{z=z_{\min}}&=0,\ u|_{z=z_{\max}}=0,\\p&=0,\end{aligned}\tag{32}$$

which represents a pipe flow in the y direction. The use of the boundary condition allows the mass conservation law to be preserved since the incompressible solvent fluid can go in and out of the simulation box freely.

B. MD/FD interface update

Once the fluid velocity field is known, the next step is to use it to update the solute/solvent interface. The equivalent step in the solute region is to update particle positions based on particle velocities. Numerically we use the level set method based on the finite-difference method.[95–97] In the level set method, a scalar function, i.e., the level set function, is used to represent the moving interface implicitly. The interface is located where the level set function is zero ($d=0$), i.e., the zero level set $\Gamma(t)=\{y:d(y,t)=0\}$. Suppose that $\Gamma(t)$ moves according to velocity v, $\partial\Gamma(t)/\partial t=v(\Gamma(t))$, where v is known after the fluid dynamics equations are solved. Given the interface velocity, if we want the level set function (d) to satisfy $\Gamma(t)=\{y:d(y,t)=0\}$ after update, we can impose the following equation upon $d(y,t)$:[95–97]

$$\frac{\partial d}{\partial t}+v\cdot\nabla d=0\tag{33}$$

with the initial condition $\Gamma(0)=\{y:d(y,0)=0\}$, i.e., the level set function initially set for the initial configuration in our case. Here the level set function was initially set as a signed distance function to the solvent accessible surface with a specified solvent probe.

C. Overview of the MD/FD numerical procedure

In our system, the atomic details for the solute region are preserved, and the solvent region is modeled as in Sec. II A. To simulate the solute particle dynamics, a standard MD engine with the leapfrog time integrator[98] coupled to a heat bath is used. The temperature coupling is realized with the Berendsen thermostat, which has been widely used in molecular simulation community.[99] Once the heat bath is specified, the procedure of the MD/FD can be summarized into the following steps:

1. Input and initialize system parameters for solute atoms such as temperature, number of particles, time step, etc. Initialize initial positions and velocities of all solute atoms.
2. Initialize FD simulation box and grid points. Initialize velocity and pressure of fluid elements.
3. Compute energy and forces from the potential function of solute atoms.
4. Compute van der Waals forces and pressure between solute atoms and fluid atoms.
5. Use the particle MD engine to update new velocities and positions of solute atoms.
6. Use the FD engine to update new velocities and pressures of fluid elements.
7. Update new MD/FD interface.
8. Repeat steps 3-7.

Dynamics variables, such as position, velocity, pressure, and level set function, are periodically stored after step 7 as requested. These can be used as input to restart the MD/FD simulation as needed.

IV. OTHER COMPUTATIONAL DETAILS

For the FD simulations, physical parameters of water are set as those at 300 K with viscosity $\mu=8.51\times10^{-4}$ Pa s, density $\rho=1.00\times10^3$ kg/m^3, and hydrophobic surface tension $\gamma=8.94\times10^{-2}$ kcal/mol Å^2, with the later optimized for biomolecules given the solvent accessible molecular surface definition in a previous work for the Amber force fields.[84] The water probe was set as 1.0 Å to set up the initial molecular surface. In the FD simulation programs, both water viscosity

TABLE I. Conversion factors between FD and MD units.

Variable	MD unit	FD unit
Time (t)	1 ps	85.1
Mass	1 kg	1.00×10^{27}
Energy (E)	1 kcal/mol	9.60×10^{-2}

and density are often set as 1.0 in the internal unit. Thus a proper interface between FD and MD simulation portions of our algorithm requires careful unit conversion. The details in deriving these conversion factors are given in the Appendix, and the actual conversion factors are listed in Table I.

The MD/FD multi-scale simulation engine was developed in a revised Amber 16 release.[65–67] The Amber *ff14* force field is used to generate the topology files and the TIP3P water is used to model the water molecules. All atomic charges were set to be zero to focus on the nonelectrostatic interactions in this study. The simulations were conducted with bonds involving hydrogen constrained via the SHAKE algorithm. The time step was set to be 0.002 ps for both the fluid dynamics region and molecule dynamics region. The temperature coupling constant is 0.2 ps in Berendsen's thermostat to couple the temperature of the MD region, which is set to be 5 K to study the relaxation of the solute-solvent interface in this study. The simulation box is four times as large as the solute dimension.

Since the goal of the current development is to evaluate how well the MD/FD method reproduces the solvent interface, the atoms in the MD region are restrained to their initial positions with a harmonic potential of force constant of 50 kcal/mol-Å to focus on the FD simulation. The initial solvent-solute interface was set as the solvent accessible surface with a solvent probe of 1.0 Å. The small probe was used as we anticipate that the final solvent-solute interface would shrink to an interface similar to the solvent excluded surface. Given that the external forces on the FD region are currently only van der Waals force and hydrophobic force, and that they should balance each other at equilibrium, we explored how to both artificially increase the external force terms (by a factor of 10) and decrease the viscosity terms (by a factor of 10) to accelerate the relaxation towards equilibrium. It was found that the low viscosity runs did not relax as fast as the high force runs (data not shown). Nevertheless all alternatives will be further explored in a future study.

A single ion (Na^+), a single molecule n-methyl amine (NMA), and four typical small molecular complexes, adenine-thymine (AT), guanine-cytosine (GC), arginine-aspartic acid (RD), and lysine-aspartic acid (KD), were chosen to analyze the solute-solvent surface produced by the new method. In this stage of our development, the electrostatic interactions were turned off so only van der Waals and hydrophobic interactions of the solute molecules were considered though water molecules were not alternated. As a benchmark to evaluate the quality of the new multi-scale algorithm, we conducted all-atom molecular mechanics simulations for the four tested dimer complexes to sample the solvent interface with explicit TIP3P water molecules. In these simulations, all molecules first underwent a 10 000-step energy minimization starting with a 5000-step steepest descent followed by a 5000-step conjugate gradient minimization. Then all solute atoms were restrained to their initial positions with a harmonic potential of force constant of 50 kcal/mol-Å in all subsequent heating, equilibration, and production simulations. The molecular dynamics simulations were first heated up from 0 K to 300 K in 20 ps. This was then followed with a 10 ns simulation at the constant temperature of 300 K and the constant pressure of 1 bar with the Berendsen heat and pressure baths. The water molecules sampled in the last 5 ns were used to analyze the solute-solvent surfaces.

V. RESULTS AND DISCUSSION

A. Single atom relaxation: Reproduction of analytical solution

We first validated the MD/FD engine with a simple system with analytical solution: the solute-solvent interface of a single atom, given that the balance of hydrophobic force and van der Waals force would lead to a final equilibrium surface. The equilibrium can be analytically solved once the solvation free energy for a van der Waals sphere of radius R is given as

$$G = \rho \int_R^{+\infty} \left(\frac{A}{r^{12}} - \frac{B}{r^6} \right) 4\pi r^2 dr + \gamma 4\pi R^2$$
$$= 4\pi\rho \left(\frac{A}{9R^9} - \frac{B}{3R^3} \right) + 4\pi\gamma R^2. \quad (34)$$

Starting from a given initial state, it is expected that the system converges to its free energy minimum if there is no energy barrier, which is the case here.

In this test, an Amber sodium ion solvated in TIP3P water was used as an illustration. With the specified surface tension and van der Waals parameters from the *ff14* force field, the gradient of the free energy can be expressed as

$$\frac{\partial G}{\partial R} = 4\pi\rho \left(-\frac{A}{R^{10}} + \frac{B}{R^4} \right) + 8\pi\gamma R. \quad (35)$$

Given the values of A = 4127 (kcal/mol)·Å^{12}, B = 3.570 (kcal/mol)·Å^6, and $\gamma = 8.94 \times 10^{-2}$ kcal/(mol·Å^2), the numerical solution shows that there is only one root for $\frac{\partial G}{\partial R} = 0$ when R is positive, which gives the radius of the sphere to be 2.45 Å. It is also clear that $\frac{\partial G}{\partial R} < 0$ when R approaches 0^+ and $\frac{\partial G}{\partial R} > 0$ when R approaches infinity. Given that (1) the gradient changes from negative to positive as r changes from 0^+ to $+\infty$ and (2) there is only one root for the gradient, it can be concluded that the gradient is negative when R < 2.45 Å and positive when R > 2.45 Å. Thus, free energy G is monotonically decreasing when R < 2.45 Å and monotonically increasing when R > 2.45 Å. This analysis shows that there is no energy barrier in the physically allowed range of R.

Therefore it is possible to use a simple steepest descent minimization or a low-temperature MD relaxation to reach the global minimum in the solvation free energy. Figure 1 plots the evolution of volume versus time for the tested low-temperature relaxation run. It is apparent that the volume of the solute-solvent interface quickly converges to a constant volume, consistent with our analysis above. The numerical volume agrees with the analytical solution with an error of

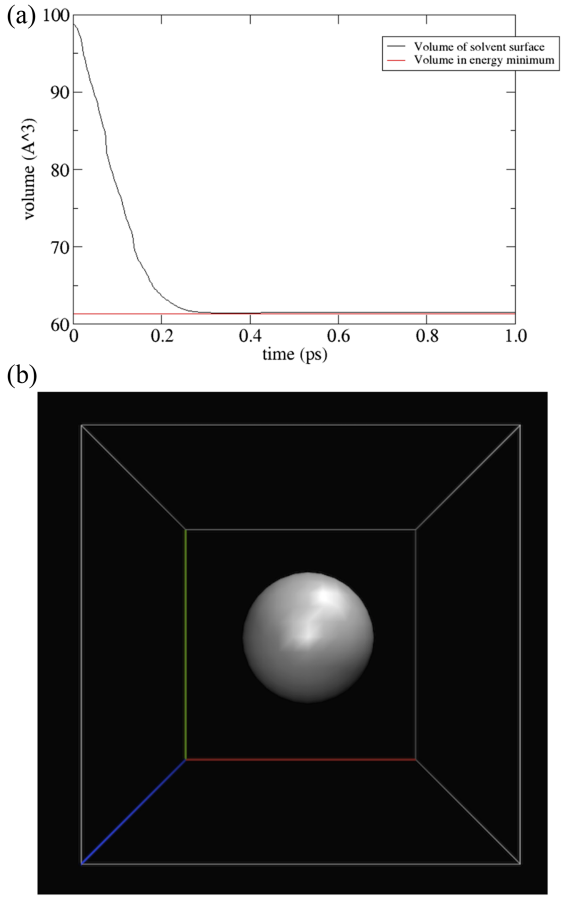

FIG. 1. (a) Time evolution of volume (Å^3) in the restrained MD/FD simulation of sodium ion. (b) Spherical contour of solute-solvent interface when reaching the equilibrium.

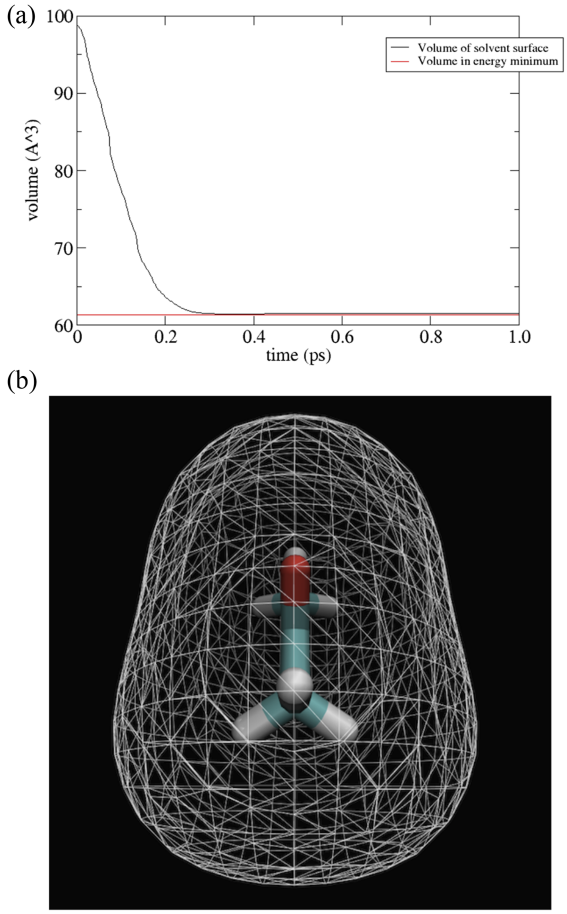

FIG. 2. (a) Time evolution of volume (Å^3) in the restrained MD/FD simulation of NMA. (b) SES-like solute-solvent interface is observed when reaching the equilibrium.

~0.3%. Note also that the equilibrium volume is a spherical sphere for the single ion as expected.

B. Monomer relaxation: Symmetric interface

Next, we performed the low-temperature relaxation of n-methyl amine, a mirror-symmetrical monomer. As shown in Fig. 2, the volume reaches the equilibrium value within 500 steps (1.0 ps). The contour plot shows that the symmetrical monomer possesses a symmetrical interface at equilibrium. VMD visualization in 3D indicates that a detailed surface contour similar to that of the solvent excluded surface can be found (see the supplementary material).

C. Dimer relaxation

Four typical small molecular complexes, adenine-thymine, guanine-cytosine, arginine-aspartic acid, and lysine-aspartic acid, were tested to evaluate the performance of the MD/FD simulation method. As shown in Fig. 3, the solute volumes reach the equilibrium values within 500 steps (1.0 ps) for all four dimers. Figure 4 presents the time evolutions of force balancing on the solute-solvent interface. It is clear that the numerical solvent pressure and viscosity pressure decrease significantly and approach zero as time goes on. On the other hand, the hydrophobic (surface tension) pressure and the analytical van der Waals pressure become the dominant components, reaching steady values while balancing each other out. This is another evidence that the system approaches equilibrium. Apparently the balance between hydrophobic and van der Waals components is not perfect, due to the presence of residual fluid flow nearby the solute. This issue will be addressed in our future refinement of the numerical algorithm to be discussed below.

D. Comparison with explicit solvent simulations

Finally, a key issue in the current development of the MD/FD algorithm is to see whether the algorithm at least qualitatively agrees with explicit solvent MD simulations. Discrepancy is possible given that no optimization has been attempted. Therefore, it is interesting to analyze the solute-solvent interfaces as sampled by both the MD/FD algorithm and the explicit solvent MD algorithm.

This analysis was conducted in the following manner. The water molecules in explicit solvent MD simulations were sampled every 5 ps over the course of a 5 ns production run for each tested dimer with all solute atoms restrained in the initial position. A total of 1000 snapshots were collected for visualization. To facilitate visualization, water molecules beyond 3.0 Å distance from any solute atom were discarded. The water distribution maps were used as references to assess the solute-solvent surface sampled by the MD/FD simulation method. Figure 5 shows the distribution of water oxygen atoms and the MD/FD surface when viewed outside of the solute-solvent

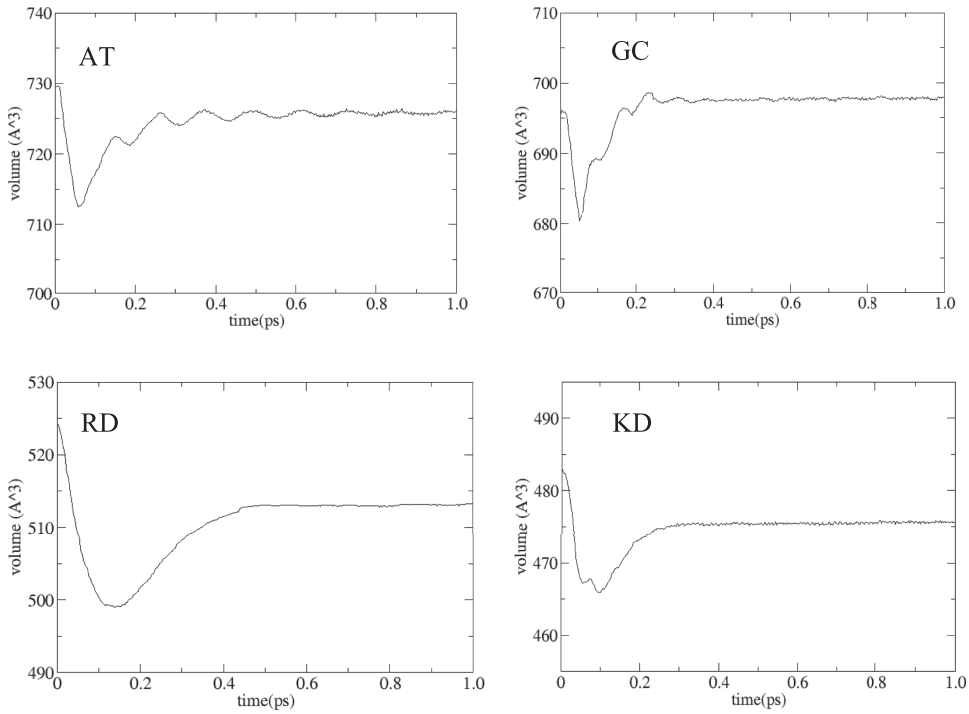

FIG. 3. Time evolutions of volume (Å^3) in the restrained MD/FD simulations of dimers: AT, GC, RD, and KD.

surface, and Fig. 6 shows the distribution and surface when viewed inside of the solute-solvent surface. Overall, the MD/FD surfaces match very well with the solute-solvent boundaries as sampled in the explicit MD simulations for all four tested complexes. Note also there are a few places of discrepancies, which indicate that the parameters used in the MD/FD algorithm need to be optimized. VMD visualization in 3D further illustrates the agreement presented here (see the supplementary material).

It is worth pointing out that water penetration into the interface region is not serious when compared with explicit solvent simulations. Switching from a full atomic model to a continuum model is bound to lose details on molecular fluctuations. The minimum in the free energy is shallow, and this suggests that for small systems, one would expect molecular fluctuations. Besides this, the concept of a molecular surface being defined by a spherical probe is an idealization of a water molecule. Thus a perfect match is probably not possible even after further optimization.

E. Limitations of the algorithm and future directions

There are clearly limitations in the proposed MD/FD algorithm. The first limitation is that we artificially make both

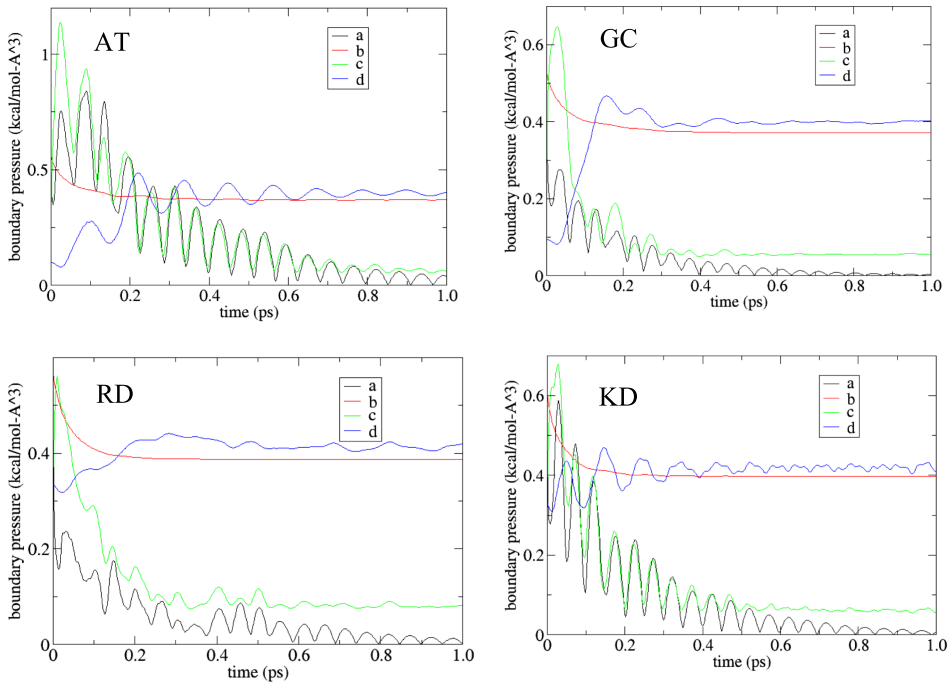

FIG. 4. Time evolutions of average absolute pressure components on the solute-solvent interface: AT, GC, RD, and KD. (a) Numerical solvent pressure. (b) Hydrophobic pressure. (c) Viscosity pressure. (d) Analytical van der Waals pressure.

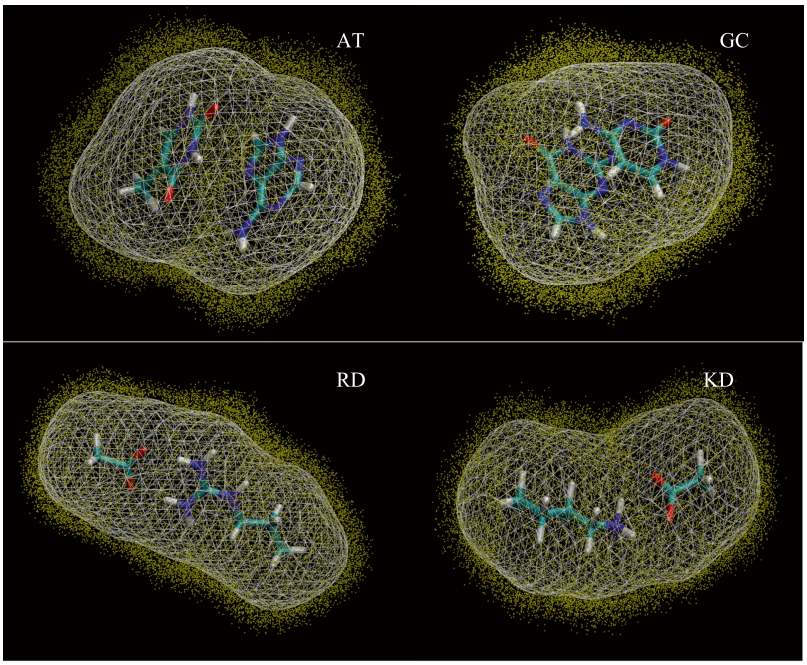

FIG. 5. MD/FD surfaces (white wireframe) and water molecules from explicit MD simulations (yellow dots) of four tested dimers: AT, GC, RD, and KD. Here the viewer stands outside of the surfaces.

hydrophobic and van der Waals terms 10 times higher to accelerate the solute-solvent interface relaxation because the focus of the current algorithm is for equilibrium properties of the solute, but not the physically correct solvation relaxation process, which may be important if the MD/FD algorithm is applied to study hydrodynamic properties due to the presence of the large molecular solute. Nevertheless, the artificial setting does not affect the converged solute-solvent interface because both hydrophobic and van der Waals pressures are simultaneously increased and the solute still feels the original hydrophobic and van der Waals terms. Second, the finite-difference grid spacing used in the FD engine is 0.5 Å, which is widely used in biomolecular applications of a finite-difference method given a high enough resolution of molecular surface topology can be achieved. However, the relatively fine grid also leads to a highly inefficient numerical procedure. To date we have not paid special attention to the numerical efficiency of our FD engine, and this will be a focus in our future development, either via accelerated FD algorithms or simplified FD schemes given that our focus is on equilibrium properties. The development and illustrations here mainly show that the MD/FD algorithm is sound and it does produce physically meaningful observations consistent with the all-atom MD algorithm, which is very promising.

As we pointed out in Sec. IV, the FD parameters for the water solvation process were from a previous study to optimize a related nonpolar solvent model. Apparently this is not optimal for the current MD/FD algorithm. Our next step will

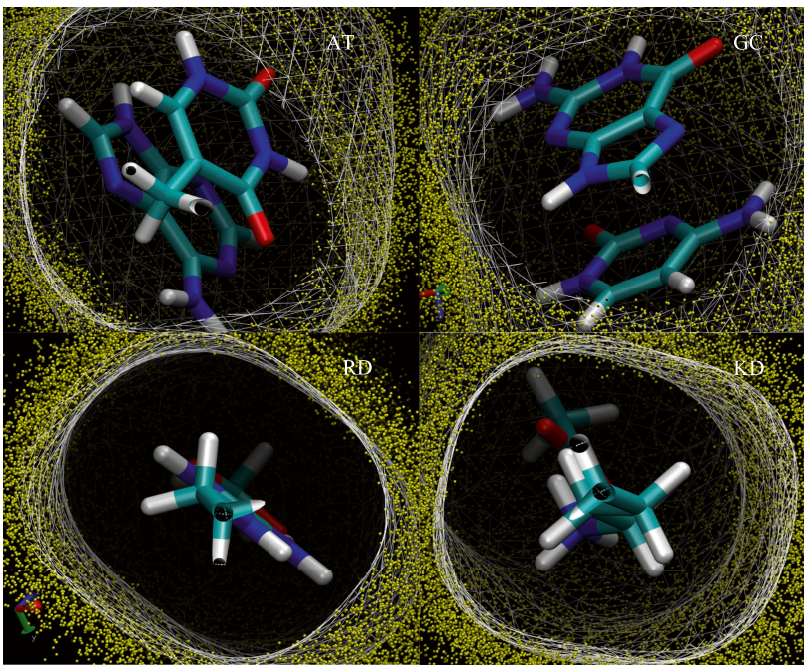

FIG. 6. MD/FD surfaces (white wireframe) and water molecules from explicit MD simulations (yellow dots) of four tested dimers: AT, GC, RD, and KD. Here the viewer stands inside of the surfaces.

be to investigate how to optimize the hydrophobic term and van der Waals term to best reproduce the all-atom explicit solvent model. In addition, we will also incorporate the electrostatic interaction as modeled by the numerical PBE method to build a more realistic MD/FD algorithm for biomolecular applications.

VI. CONCLUSIONS

In this study, we explored a multi-scale algorithm for the Poisson-Boltzmann continuum solvent model for more robust simulations of biomolecules. This method utilizes a recently developed fluid dynamics algorithm to simulate the continuum solvent/solute interface, which is tightly coupled to the solute molecular dynamics simulation realized with the Amber molecular mechanics engine.[65–67] A major issue in the application of the multi-scale algorithm in atomistic simulations is the presence of van der Waals potential, which has a large gradient nearby the solute-solvent interface. It is virtually impossible to treat van der Waals potentials with any reasonably fine finite-difference method. We overcame the challenge by removing the van der Waals potential from pressure when solving the finite-difference fluid dynamics equations and adding back the van der Waals potential analytically in the free-boundary condition.

We first validated the MD/FD engine with a simple system with analytical solution: the solute-solvent interface of a single atom. The balance of hydrophobic force and van der Waals force would lead to the final equilibrium surface of a sphere. Our test shows that the volume of the solute-solvent interface quickly converges to the analytical value with an error ~0.3%. Next, we performed the relaxation of NMA, a mirror-symmetrical monomer. The contour plot shows that the symmetrical monomer possesses a symmetrical interface at equilibration. VMD visualization in 3D indicates that a detailed surface contour similar to that of the solvent excluded surface can be found. Four typical molecular complexes were then tested to evaluate the performance of the MD/FD simulation method. The solute volumes reach the equilibrium values within 1.0 ps for all four dimers. The time evolutions of force balancing analysis on the solute-solvent interface show that the numerical solvent pressure and viscosity pressure decrease significantly and approach zero as simulation time goes on. On the other hand, the hydrophobic (surface tension) pressure and the analytical van der Waals pressure become the dominant components, reaching steady values while balancing each other out. This strongly indicates that the systems approach the equilibrium at the end of the simulations.

Finally, a key issue at the current stage of the development is to investigate whether the algorithm at least qualitatively agrees with explicit solvent MD simulations. Therefore, it is interesting to analyze the solute-solvent interfaces as sampled by both the MD/FD method and the explicit solvent MD method. Comparisons show that the MD/FD surfaces agree very well with the solute-solvent boundaries as sampled in the explicit MD simulations for all four tested dimers. Note also that a few places of discrepancies do exist, which indicates that the parameters used in the MD/FD method need to be optimized further to achieve higher consistency with the all-atom explicit solvent MD method.

In our next phase of the development, we will further improve the quality of hydrophobic and van der Waals terms of the FD procedure to best reproduce all-atom simulations. In addition it is important to investigate the effect of incorporating, the electrostatic forces into the MD/FD algorithm to evaluate its impact on both numerical stability and consistency for a range of model systems. Finally it is interesting to explore more efficient and/or simplified numerical FD engines for routine applications to biomolecular systems.

SUPPLEMENTARY MATERIAL

See supplementary material for the 3D visualization in VMD for monomer NMA and the four molecular dimer complexes: adenine-thymine (AT), guanine-cytosine (GC), arginine-aspartic acid (RD), and lysine-aspartic acid (KD).

ACKNOWLEDGMENTS

We are grateful for the insightful critiques of an anonymous reviewer at JCP. Incorporation of these critiques greatly improved the quality and clarity of the manuscript before publication. This work was supported in part by NIH/NIGMS (Nos. GM093040 and GM079383).

APPENDIX: DERIVATION OF CONVERSION FACTORS BETWEEN MD AND FD UNITS

Since FD programs can use any arbitrary length unit, we set 1 internal length unit as 1 Å. Given the length unit settled and the water density ($\rho = 1.00 \times 10^3$ kg/m^3) set as 1 internal density unit, the internal mass unit can be computed to be equivalent to 1.00×10^{-27} kg. Next we can utilize viscosity to compute the time conversion factor. Given the unit of viscosity Pa s = kg/(m s) we can use the mass conversion factor to derive the time conversion factor as follows:

$$\begin{aligned} 1 \text{ internal viscosity unit} &= 8.509 \times 10^{-4} \text{ kg/(m} \cdot \text{s)} \\ &= 8.509 \times 10^{-4} \times 1.00 \\ &\quad \times 10^{27}/(10^{10} \times T). \end{aligned} \tag{A1}$$

This leads to $T = 8.51 \times 10^{13}$, which means 1 s = 8.51×10^{13} internal time unit. And thus we have 1 ps = 10^{-12} s = 85.1 internal time unit. The energy unit of 1 kcal/mol can be converted as

$$\begin{aligned} 1 \text{ kcal/mol} &= 6.948 \times 10^{-21} \text{ J} = 6.948 \times 10^{-21} \text{ kg m}^2/\text{s}^2 \\ &= 6.948 \times 10^{-21} \times 10^{27} \\ &\quad \times (10^{10})^2/(8.509 \times 10^{13})^2 \text{ internal energy unit} \\ &= 9.60 \times 10^{-2} \text{ internal energy unit.} \end{aligned} \tag{A2}$$

[1] M. E. Davis and J. A. McCammon, Chem. Rev. **90**, 509 (1990).
[2] B. Honig, K. Sharp, and A. S. Yang, J. Phys. Chem. **97**, 1101 (1993).
[3] B. Honig and A. Nicholls, Science **268**, 1144 (1995).
[4] D. Beglov and B. Roux, J. Chem. Phys. **104**, 8678 (1996).
[5] C. J. Cramer and D. G. Truhlar, Chem. Rev. **99**, 2161 (1999).
[6] D. Bashford and D. A. Case, Annu. Rev. Phys. Chem. **51**, 129 (2000).

[7]N. A. Baker, Curr. Opin. Struct. Biol. **15**, 137 (2005).
[8]J. H. Chen, W. P. Im, and C. L. Brooks, J. Am. Chem. Soc. **128**, 3728 (2006).
[9]M. Feig, J. Chocholousova, and S. Tanizaki, Theor. Chem. Acc. **116**, 194 (2006).
[10]P. Koehl, Curr. Opin. Struct. Biol. **16**, 142 (2006).
[11]W. Im, J. H. Chen, and C. L. Brooks, Adv. Protein Chem. **72**, 173 (2006).
[12]B. Z. Lu, Y. C. Zhou, M. J. Holst, and J. A. McCammon, Commun. Comput. Phys. **3**, 973 (2008).
[13]J. Wang, C. H. Tan, Y. H. Tan, Q. Lu, and R. Luo, Commun. Comput. Phys. **3**, 1010 (2008).
[14]M. D. Altman, J. P. Bardhan, J. K. White, and B. Tidor, J. Comput. Chem. **30**, 132 (2009).
[15]Q. Cai, J. Wang, M.-J. Hsieh, X. Ye, and R. Luo, in *Annual Reports in Computational Chemistry*, edited by A. W. Ralph (Elsevier, 2012), p. 149.
[16]L. Xiao, C. Wang, and R. Luo, J. Theor. Comput. Chem. **13**, 1430001 (2014).
[17]W. M. Botello-Smith, Q. Cai, and R. Luo, J. Theor. Comput. Chem. **13**, 1440008 (2014).
[18]R. E. Georgescu, E. G. Alexov, and M. R. Gunner, Biophys. J. **83**, 1731 (2002).
[19]J. E. Nielsen and J. A. McCammon, Protein Sci. **12**, 313 (2003).
[20]J. Warwicker, Protein Sci. **13**, 2793 (2004).
[21]C. L. Tang, E. Alexov, A. M. Pyle, and B. Honig, J. Mol. Biol. **366**, 1475 (2007).
[22]J. M. J. Swanson, R. H. Henchman, and J. A. McCammon, Biophys. J. **86**, 67 (2004).
[23]C. Bertonati, B. Honig, and E. Alexov, Biophys. J. **92**, 1891 (2007).
[24]A. R. Brice and B. N. Dominy, J. Comput. Chem. **32**, 1431 (2011).
[25]R. Luo, H. S. R. Gilson, M. J. Potter, and M. K. Gilson, Biophys. J. **80**, 140 (2001).
[26]L. David, R. Luo, M. S. Head, and M. K. Gilson, J. Phys. Chem. B **103**, 1031 (1999).
[27]D. Shivakumar, Y. Q. Deng, and B. Roux, J. Chem. Theory Comput. **5**, 919 (2009).
[28]A. Nicholls, D. L. Mobley, J. P. Guthrie, J. D. Chodera, C. I. Bayly, M. D. Cooper, and V. S. Pande, J. Med. Chem. **51**, 769 (2008).
[29]T. P. Korman, Y.-H. Tan, J. Wong, R. Luo, and S.-C. Tsai, Biochemistry **47**, 1837 (2008).
[30]R. Luo, M. S. Head, J. A. Given, and M. K. Gilson, Biophys. Chem. **78**, 183 (1999).
[31]K. L. Mardis, R. Luo, and M. K. Gilson, J. Mol. Biol. **309**, 507 (2001).
[32]S. A. Marshall, C. L. Vizcarra, and S. L. Mayo, Protein Sci. **14**, 1293 (2005).
[33]M. J. Hsieh and R. Luo, Proteins: Struct., Funct., Bioinf. **56**, 475 (2004).
[34]E. Z. Wen and R. Luo, J. Chem. Phys. **121**, 2412 (2004).
[35]E. Z. Wen, M. J. Hsieh, P. A. Kollman, and R. Luo, J. Mol. Graphics Modell. **22**, 415 (2004).
[36]T. Z. Lwin and R. Luo, J. Chem. Phys. **123**, 194904 (2005).
[37]T. Z. Lwin, R. H. Zhou, and R. Luo, J. Chem. Phys. **124**, 034902 (2006).
[38]T. Z. Lwin and R. Luo, Protein Sci. **15**, 2642 (2006).
[39]Y.-H. Tan and R. Luo, J. Phys. Chem. B **112**, 1875 (2008).
[40]Y. Tan and R. Luo, PMC Biophys. **2**, 5 (2009).
[41]Q. Lu, Y.-H. Tan, and R. Luo, J. Phys. Chem. B **111**, 11538 (2007).
[42]J. Wang, C. Tan, H.-F. Chen, and R. Luo, Biophys. J. **95**, 5037 (2008).
[43]J. Warwicker and H. C. Watson, J. Mol. Biol. **157**, 671 (1982).
[44]D. Bashford and M. Karplus, Biochemistry **29**, 10219 (1990).
[45]A. Jeancharles, A. Nicholls, K. Sharp, B. Honig, A. Tempczyk, T. F. Hendrickson, and W. C. Still, J. Am. Chem. Soc. **113**, 1454 (1991).
[46]M. K. Gilson, Curr. Opin. Struct. Biol. **5**, 216 (1995).
[47]S. R. Edinger, C. Cortis, P. S. Shenkin, and R. A. Friesner, J. Phys. Chem. B **101**, 1190 (1997).
[48]C. Tan, L. Yang, and R. Luo, J. Phys. Chem. B **110**, 18680 (2006).
[49]Q. Cai, J. Wang, H.-K. Zhao, and R. Luo, J. Chem. Phys. **130**, 145101 (2009).
[50]J. Wang, Q. Cai, Z.-L. Li, H.-K. Zhao, and R. Luo, Chem. Phys. Lett. **468**, 112 (2009).
[51]X. Ye, Q. Cai, W. Yang, and R. Luo, Biophys. J. **97**, 554 (2009).
[52]X. Ye, J. Wang, and R. Luo, J. Chem. Theory Comput. **6**, 1157 (2010).
[53]R. Luo, J. Moult, and M. K. Gilson, J. Phys. Chem. B **101**, 11226 (1997).
[54]J. Wang, C. Tan, E. Chanco, and R. Luo, Phys. Chem. Chem. Phys. **12**, 1194 (2010).
[55]M. J. Hsieh and R. Luo, J. Mol. Model. **17**, 1985 (2011).
[56]Q. Cai, X. Ye, J. Wang, and R. Luo, J. Chem. Theory Comput. **7**, 3608 (2011).
[57]J. Wang, Q. Cai, Y. Xiang, and R. Luo, J. Chem. Theory Comput. **8**, 2741 (2012).
[58]X. Liu, C. Wang, J. Wang, Z. Li, H. Zhao, and R. Luo, Phys. Chem. Chem. Phys. **15**, 129 (2013).
[59]C. Wang, J. Wang, Q. Cai, Z. L. Li, H. Zhao, and R. Luo, Comput. Theor. Chem. **1024**, 34 (2013).
[60]L. Xiao, Q. Cai, X. Ye, J. Wang, and R. Luo, J. Chem. Phys. **139**, 094106 (2013).
[61]M. Ozboyaci, D. B. Kokh, S. Corni, and R. C. Wade, Q. Rev. Biophys. **49**, e4 (2016).
[62]M. Valtiner, A. Erbe, and A. Rosenhahn, Biointerphases **11**, 018801 (2016).
[63]L. Xiao, Q. Cai, Z. Li, H. Zhao, and R. Luo, Chem. Phys. Lett. **616-617**, 67 (2014).
[64]Z. L. Li, L. Xiao, Q. Cai, H. K. Zhao, and R. Luo, J. Comput. Phys. **297**, 182 (2015).
[65]D. A. Case, R. M. Betz, W. Botello-Smith, D. S. Cerutti, I. T. E. Cheatham, T. A. Darden, R. E. Duke, T. J. Giese, H. Gohlke, A. W. Goetz, N. Homeyer, S. Izadi, P. Janowski, J. Kaus, A. Kovalenko, T. S. Lee, S. LeGrand, P. Li, C. Lin, T. Luchko, R. Luo, B. Madej, D. Mermelstein, K. M. Merz, G. Monard, H. Nguyen, H. T. Nguyen, I. Omelyan, A. Onufriev, D. R. Roe, A. Roitberg, C. Sagui, C. L. Simmerling, J. Swails, R. C. Walker, J. Wang, R. M. Wolf, X. Wu, L. Xiao, D. M. York, and P. A. Kollman, AMBER 16, University of California, San Francisco, 2016.
[66]D. A. Case, R. M. Betz, W. Botello-Smith, D. S. Cerutti, I. T. E. Cheatham, T. A. Darden, R. E. Duke, T. J. Giese, H. Gohlke, A. W. Goetz, N. Homeyer, S. Izadi, P. Janowski, J. Kaus, A. Kovalenko, T. S. Lee, S. LeGrand, P. Li, C. Lin, T. Luchko, R. Luo, B. Madej, D. Mermelstein, K. M. Merz, G. Monard, H. Nguyen, H. T. Nguyen, I. Omelyan, A. Onufriev, D. R. Roe, A. Roitberg, C. Sagui, C. L. Simmerling, J. Swails, R. C. Walker, J. Wang, R. M. Wolf, X. Wu, L. Xiao, D. M. York, and P. A. Kollman, AmberTools 16, University of California, San Francisco, 2016.
[67]D. A. Case, T. E. Cheatham, T. Darden, H. Gohlke, R. Luo, K. M. Merz, A. Onufriev, C. Simmerling, B. Wang, and R. J. Woods, J. Comput. Chem. **26**, 1668 (2005).
[68]P. K. Weiner and P. A. Kollman, J. Comput. Chem. **2**, 287 (1981).
[69]S. J. Weiner, P. A. Kollman, D. A. Case, U. C. Singh, C. Ghio, G. Alagona, S. Profeta, and P. Weiner, J. Am. Chem. Soc. **106**, 765 (1984).
[70]W. D. Cornell, P. Cieplak, C. I. Bayly, I. R. Gould, K. M. Merz, D. M. Ferguson, D. C. Spellmeyer, T. Fox, J. W. Caldwell, and P. A. Kollman, J. Am. Chem. Soc. **117**, 5179 (1995).
[71]J. M. Wang, P. Cieplak, and P. A. Kollman, J. Comput. Chem. **21**, 1049 (2000).
[72]Y. Duan, C. Wu, S. Chowdhury, M. C. Lee, G. M. Xiong, W. Zhang, R. Yang, P. Cieplak, R. Luo, T. Lee, J. Caldwell, J. M. Wang, and P. Kollman, J. Comput. Chem. **24**, 1999 (2003).
[73]L. J. Yang, C. H. Tan, M. J. Hsieh, J. M. Wang, Y. Duan, P. Cieplak, J. Caldwell, P. A. Kollman, and R. Luo, J. Phys. Chem. B **110**, 13166 (2006).
[74]B. R. Brooks, R. E. Bruccoleri, B. D. Olafson, D. J. States, S. Swaminathan, and M. Karplus, J. Comput. Chem. **4**, 187 (1983).
[75]A. D. MacKerell, D. Bashford, M. Bellott, R. L. Dunbrack, J. D. Evanseck, M. J. Field, S. Fischer, J. Gao, H. Guo, S. Ha, D. Joseph-McCarthy, L. Kuchnir, K. Kuczera, F. T. K. Lau, C. Mattos, S. Michnick, T. Ngo, D. T. Nguyen, B. Prodhom, W. E. Reiher, B. Roux, M. Schlenkrich, J. C. Smith, R. Stote, J. Straub, M. Watanabe, J. Wiorkiewicz-Kuczera, D. Yin, and M. Karplus, J. Phys. Chem. B **102**, 3586 (1998).
[76]N. Foloppe and A. D. J. MacKerell, J. Comput. Chem. **21**, 86 (2000).
[77]W. L. Jorgensen and J. Tiradorives, J. Am. Chem. Soc. **110**, 1657 (1988).
[78]W. L. Jorgensen, D. S. Maxwell, and J. TiradoRives, J. Am. Chem. Soc. **118**, 11225 (1996).
[79]G. A. Kaminski, R. A. Friesner, J. Tirado-Rives, and W. L. Jorgensen, J. Phys. Chem. B **105**, 6474 (2001).
[80]E. S. Reiner and C. J. Radke, J. Chem. Soc., Faraday Trans. **86**, 3901 (1990).
[81]K. A. Sharp and B. Honig, J. Phys. Chem. **94**, 7684 (1990).
[82]D. Chandler, Nature **437**, 640 (2005).
[83]J. Dzubiella, J. M. J. Swanson, and J. A. McCammon, Phys. Rev. Lett. **96**, 087802 (2006).
[84]C. Tan, Y. H. Tan, and R. Luo, J. Phys. Chem. B **111**, 12263 (2007).
[85]L. T. Cheng, J. Dzubiella, J. A. McCammon, and B. Li, J. Chem. Phys. **127**, 084503 (2007).
[86]P. W. Bates, Z. Chen, Y. H. Sun, G. W. Wei, and S. Zhao, J. Math. Biol. **59**, 193 (2009).
[87]B. D. Jones, preprint arXiv:1407.1035v1 (2014).

[88]A. L. Fetter and J. D. Walecka, *Theoretical Mechanics of Particles and Continua* (Dover Publications, Inc., Mineola, New York, 2003).
[89]R. Car and M. Parrinello, Phys. Rev. Lett. **55**, 2471 (1985).
[90]Z. L. Li, M. C. Lai, G. W. He, and H. K. Zhao, Comput. Fluids **39**, 1033 (2010).
[91]J. Wang and R. Luo, J. Comput. Chem. **31**, 1689 (2010).
[92]Q. Cai, M.-J. Hsieh, J. Wang, and R. Luo, J. Chem. Theory Comput. **6**, 203 (2010).
[93]R. Luo, L. David, and M. K. Gilson, J. Comput. Chem. **23**, 1244 (2002).
[94]Q. Lu and R. Luo, J. Chem. Phys. **119**, 11035 (2003).
[95]S. Osher and J. Sethian, J. Comput. Phys. **79**, 12 (1988).
[96]J. A. Sethian, *Level Set Methods and Fast Marching Methods* (Cambridge University Press, Cambridge, 1999).
[97]S. Osher and R. Fedkiw, *Level Set Methods and Dynamic Implicit Surfaces* (Springer, Berlin, 2002).
[98]R. W Hockney and J. W. Eastwood, *Computer Simulations Using Particles* (Taylor & Francis, New York, 1988).
[99]H. J. C. Berendsen, J. P. M. Postma, W. F. v. Gunsteren, A. DiNola, and J. R. Haak, J. Chem. Phys. **81**, 3684 (1984).